

USE OF HORIZONTAL GRADIENT AND ANALYTICAL SIGNAL OF GRAVITY DATA FOR IDENTIFYING THE SUBSURFACE STRUCTURAL SETTING IN WADI EL-ASSUITY AREA, EGYPT

A.S. Helaly

Department of Geophysics, Faculty of Science, Ain Shams University, Abbassia, Cairo, Egypt, 11566

E.mail: Ahmad.Helaly@geologist.com

إستخدام الإنحدار الأفقى والعلامة التحليلية لبيانات الجاذبية فى التعرف على الوضع التركيبى فى منطقة وادى الأسيوطى، مصر

الخلاصة: يقع وادى الأسيوطى فى الجزء الأوسط من الصحراء الشرقية - مصر. فى هذه الدراسة- فإن المؤلف حاول تحديد ورسم التراكيب التحتسطحية العميقة من خلال تفسير بيانات الجاذبية. تقنيات الإنحدار الأفقى والعلامة التحليلية أستخدمت فى هذه الدراسة. أشارت البيانات إلى أن المنطقة تتميز بوجود ارتفاع فى الانحدار مما يعكس وجود حالات شاذة خطية من العناصر التركيبية فى شكل الصدوع التى تضرب أساسا فى إتجاه شمال شرق - جنوب غرب - داخل وادى الأسيوطى - وتضرب شمال غرب - جنوب شرق - فى وادى النيل. الحوض الذى يتجه شمال شرق فى منطقة وادى الأسيوطى يغير إتجاهه ليكون متجها شمال غرب فى منطقة وادى النيل. تحديد إتجاه المضرب الجيولوجى يكون أدق من خلال تفسير سعة العلامة التحليلية عن معلومات المجال الأسمى ويساعد على تحديد أعماق التراكيب من خلال قياس المسافة الأفقية بين نقطتى الحدود الدنيا للإشارة التحليلية الشاذة. وقد قدرت الأعماق لهذه الفواصل أو الصدوع فيما بين ٤,٨ و ٥,٨ كيلومترات. الإنحدار التفاضلى الواسع فى الجزء الشمال الشرقى بمنطقة الدراسة تم تقسيمه إلى عدد من الفوالق ذات إتجاهات رمى مختلفة وتم رسم نموذج مفاهيمى فى إتجاه شمال غرب- جنوب شرق ليمثل تقريبا الوضع التركيبى العميق فى منطقة الدراسة.

ABSTRACT: Wadi El-Assuity is located in the central part of the Eastern Desert, Egypt. In this study, the author attempted to delineate the relatively deep subsurface structures of the area through the interpretation of the available Bouguer gravity data. The horizontal gradient and analytical signal techniques were applied in the present study. Interpretation of horizontal gradient of the gravity data indicated that, the area is characterized by the existence of high gradient anomalies reflecting the presence of linear structural elements in the form of faults that are mainly striking in the NE-SW direction inside Wadi El-Assuity and NW-SE direction in the Nile Valley. The NE oriented fault bounding the southeastern side of El-Assuity coalesces with a zigzag fault system that extends to the Western Desert. The NE elongated graben in Wadi El-Assuity changes its trend to have NW-SE direction inside the Nile Valley. The direction of a geologic strike is easier to deal with through the interpretation of analytical signal amplitude than of the original field data. It is also straight forward to determine the depths to causative sources from the distance between minima points of analytical signal anomalies. Therefore, the analytical signal was used to estimate the depths to such deep contacts, which range from 4.8 to 5.8 km. The wide gravity gradient in the study area was inspected into a number of expected fault elements of different throw directions, based on the analysis of the analytical signal method. Based on the estimated depths and slightly varying density contrasts, a conceptual model along one profile was introduced to represent the expected general deep structural set-up in the area under study.

Keywords: Horizontal gradient, analytical signal, gravity interpretation, Wadi El-Assuity area.

INTRODUCTION

This work presents the use/importance of some potential techniques (gravity) in defining the deep structural set-up in any area. The area under study is located within the tract bounded by latitudes 27°00'00'' & 27°30'00'' and longitudes 31°00'00'' & 31°30'00'' (Fig.1). It comprises Wadi El-Assuity area, to the east of the Nile River. In this work, the gravity data represented by the Bouguer gravity anomaly map (EGPC, 1977), were used solely to decipher the deep and hidden contacts in this area. The horizontal gradient and analytical signal techniques were used to map the structural elements intervening the subsurface section.

The observed tectonic trends on the surface of this area are represented by the NW-SE lineaments, of

which the Nile River has been presented. The other lineament trends are parallel and sub-parallel to the Red Sea. A plateau of the Eocene limestone occupies the area and is characterized by low relief topography with a general inclination towards the western direction (Said, 1962). Elevations of the plateau range between 210 and 280 meters above sea level and shows on its eastern side a sharp scarp facing the Nile Valley area. Omara and El-Tahlawi (1972) recorded NW-SE, NE-SW and few N-S and E-W sedimentary dykes dissecting the Eocene limestone plateau around Assiut. Youssef et al. (1994) reported that, the NW-SE faults affecting the Eocene rocks around Assiut were developed by the post-Eocene movement. Also, the study area has been

focused by many workers (Bakheit, 1989, Youssef et al., 1994 and Attia, 1995).

Moreover, great efforts have been made to explore the Nile Valley, especially the middle part for oil and gas occurrences to delineate the historical places such as temples, to establish new industries, as well as big economic projects and to construct new cities along the plateau surrounding the Nile Valley (Abdel-Monem et al, 2004). Consequently, due to the importance of this area, some light should be thrown on its local tectonics, as well as its crustal deformations, in order to understand the general geologic set-up of the study area.

GEOLOGIC SETTING

The geologic setting of the Nile Valley attracted the attention of many researchers. The southern and northern portions of the Nile River Valley differ greatly. To the South, the valley is narrow, and the river and the fertile land on either side may only be a couple of miles in width. To the North, however, the Nile branches out forming a wide and rich delta, which together with the Fayum Oasis, forms the majority of the agricultural land in the country. This differentiation between the two parts of Egypt is shown in terms of Upper Egypt and Lower Egypt. Upper Egypt is the land upriver and Lower Egypt is the Delta region. The study area is located within the inbetween zone and with what is called Middle portion of the Nile Valley. These terms are also useful, as the Delta is geologically lower than Upper Egypt.

Generally, the Nile Valley is a structurally and erosionally controlled basin cutting through the limestone plateau. Said (1981) mentioned that, the Nile Valley was excavated during the Late Miocene age. In Assuit area, as most of the Nile Valley along the Nile River, the valley is filled with Pliocene and Quaternary deposits, bordered by the walls of Eocene limestone.

The NW elongated Nile Valley rift is differentiated into four rift segments by Abd-Allah (2008). These segments are separated by three E-W and NE striking transfer zones, which are E-W Kom Ombo-Nuqra zone, NE Qena bend zone and NE Asyut zone.

The study area attracted the author’s attention, due to the distribution of the Bouguer gravity gradients in Wadi El’Assuity area, which show a NE-SW trend intersecting with dominant NW-SE trend. Also, Figure (2) shows some NE-SW indications that may have its implications on the formation of Wadi El-Assuity with its current overall trend.

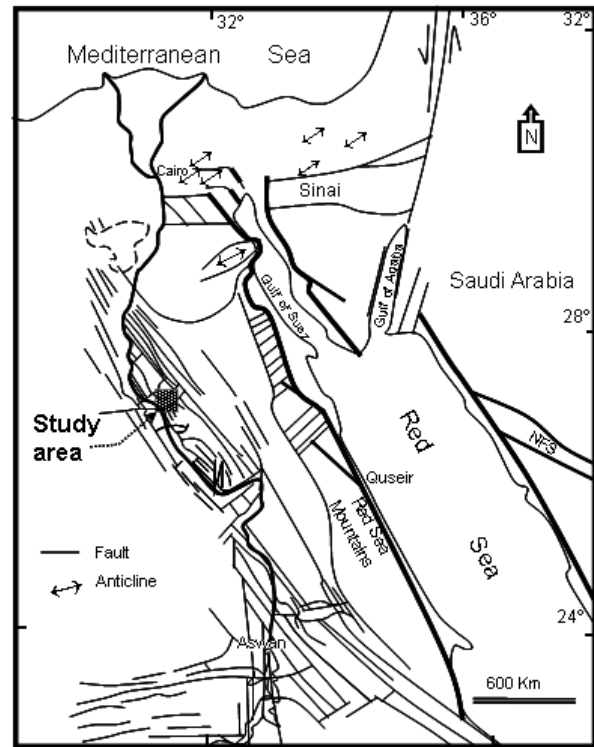


Figure 1: Location map for the study area showing the main structural features of Egypt (after Abd-Allah, 2008).

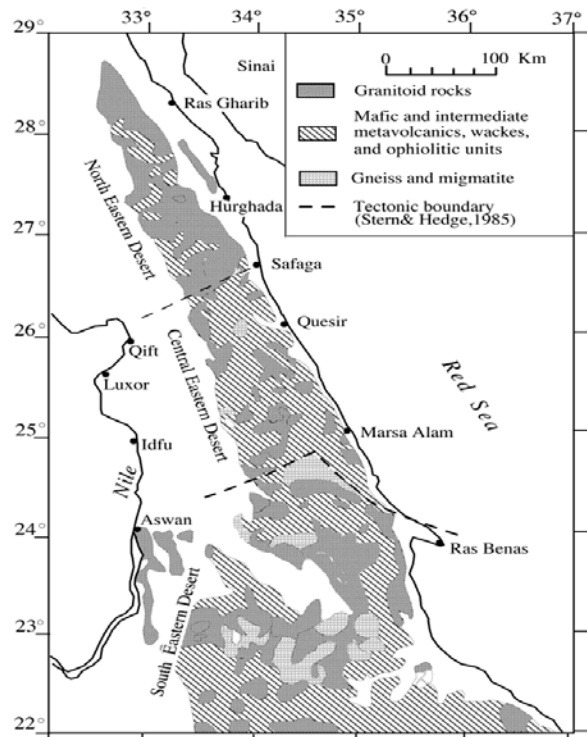


Figure 2: Outcropped Basement rocks in Eastern Desert near the study area showing NE-SW tectonic trend that might affected the study area (Stern and Hedge, 1985)

SCOPE OF THE STUDY

The goal of this study is to estimate the depths to the deep faults/contacts that affect the rocks and delimit their lateral extent, which is important to understand the overall structural set-up of the area. Surface mapping of these faults is difficult due to their great depths, beside the widespread cover of eolian sands and alluvium deposits. Drill-hole information provides a reasonable understanding of the subsurface conditions, however, this information is sparse and most of it lie outside the studied area.

Several analytical techniques have been applied to locate geologic boundaries and contacts using gravity data. Horizontal gradient analysis of gravity data is a powerful tool that helps delineating the vertical and lateral locations of the edges of the target features. Cordell (1979) and Cordell and Grauch (1985) used the maximum amplitudes of the horizontal gradients (without the vertical gradient) to locate the near-vertical geologic boundaries from gravity or pseudo-gravity anomalies. In essence, the horizontal gradient method is a special case of the use of the analytical signal, where the gravity anomaly is equivalent to the vertical magnetization anomaly from the same causative features through Poisson's relationship (Baranov, 1957). In this case, even if we do not add the vertical gradient in computing the amplitude of the analytical signal, in the absence of interference, the resulting amplitude (a bellshaped function) also has its maximum value directly over the abrupt boundaries (Nabighian, 1972).

DATA ANALYSIS

Gravity Data:

The gravity data used in this work involves the Bouguer gravity anomaly map (original scale of 1:100,000; provided by EGPC, 1977), as shown in Fig (3). The Bouguer gravity values in the study area range from -5 milligals (at the middle zone of the northern part) to -51 milligals in the central zone of the southern half of the study area. Such large closed negative anomaly (-51 milligals) represents a major gravity low. Visual inspection of Figure (3) shows that, the area is characterized by low gravity zone (ranging from -50 to -40 milligals) of a delta shape, where its base is almost parallel to the Nile River structural trend. The apex of this triangular delta-shaped contour area extends northeast-southwest. This negative, delta-shaped low, gravity zone is surrounded from all directions by lesser negative gravity gradients till the northern part of the study area, where the gravity values reach about -10 milligals or less. Diagonally, the gravity gradients in the northeastern half of the study area is characterized by a general northeast-southwest trend, while the southwestern half is portrayed by a general contour trend of northwest-southeast direction. The largest negatively-dominated zone within the central part of the

study area may reflect a graben-type feature within the sedimentary section overlying the basement rocks.

METHODOLOGY

1) Horizontal Gradient Method:

For delineating the subsurface linear structures, some of the filters can be applied, for example, the X-gradient, Y-gradient and the combined horizontal gradient magnitude.

Horizontal derivatives, which can easily be computed in the space domain, are now the most common method for detecting target edges. Cordell (1979) first demonstrated that, peaks in the magnitude of the total horizontal gradient of gravity data (square root of the sum of squares of the x - and y -derivatives) could be used to map the near-vertical boundaries of contrasting densities, such as faults and geologic contacts.

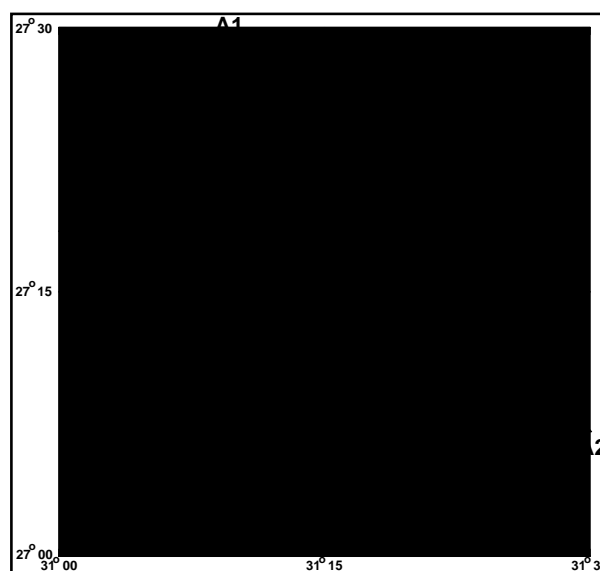


Figure 3: Bouguer Anomaly Map

The horizontal gradient method has been used intensively to locate contacts of observable density contrast from gravity data (Cordell, 1979) or pseudo-gravity data (Cordell and Grauch, 1985). Blakely and Simpson (1986) developed a useful method for gridded data, automatically locating and plotting the maxima of the horizontal gradient magnitudes. Thurston and Brown (1994) have developed convolution operators for controlling the frequency content of the horizontal derivatives and, thus, of the resulting edges. Blakely (1995) stated that, "the horizontal derivative of gravity anomalies is maximum over the boundaries of geological structures like horst or graben, masses extending horizontally and vertically, fault blocks and volcanic intrusive bodies". Blakely (1995) further stated that "the horizontal gradient of gravity anomaly caused by a tabular body tends to overlie the edges of the body, if the edges are vertical and well separated from each other". A method by Pearson (2001) finds breaks in the

horizontal derivative direction by applying a moving-window artificial intelligence operator. Cooper and Cowan (2003) introduced the combination of visualization techniques and fractional horizontal gradients to more precisely highlight subtle features of interest. A similar technique is skeletonization (Eaton and Vasudevan, 2004); this produces both an image and a database of each lineament element, which can be sorted and decimated by length or azimuth criteria.

So, fault zones associated with the formation of the basin can be determined by computing the horizontal gradient of gravity anomalies. Figure (4) illustrates the advantage of the Horizontal Gradient technique in resolving the boundaries of a source structure. Thus, the boundaries of buried vertical structures are imaged. These lineaments indicate the boundaries of the geological structures and volcanic uplifted areas. The gravity derivative map assists in the basin modelling study.

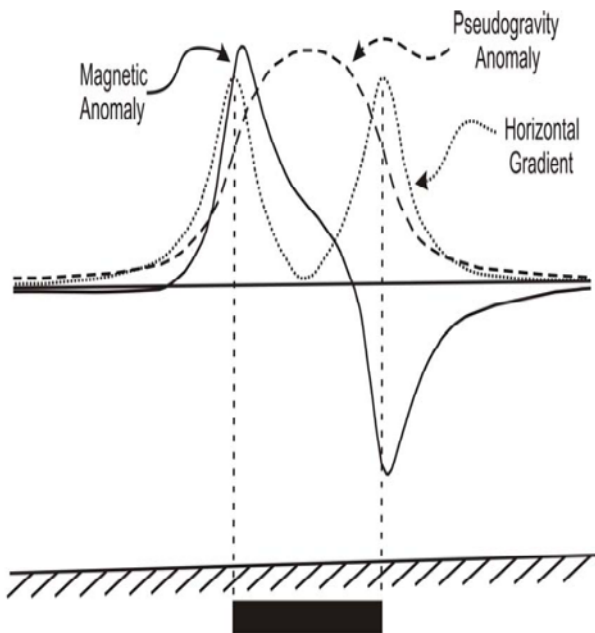


Figure 4: Magnetic anomaly, pseudo-gravity anomaly, and, horizontal gradient of the source structure (Blakely, 1995)

The biggest advantage of the horizontal gradient method is its least susceptibility to the noise in the data, because it requires only the calculations of the two first-order horizontal derivatives of the field (Phillips, 1998). The method is also robust to delineation either shallow or deep in comparison with the vertical gradient, which is useful only for the shallower structures.

The amplitude of the horizontal gradient (Cordell and Grauch, 1985) is expressed as:

$$HG = \sqrt{\left(\frac{\partial g}{\partial x}\right)^2 + \left(\frac{\partial g}{\partial y}\right)^2} \quad (1)$$

Where: $\frac{\partial g}{\partial x}$ and $\frac{\partial g}{\partial y}$ are the horizontal derivatives of the gravity field in the X and Y directions.

The map showing the distribution of horizontal gradient values is illustrated in Figure (5). High gradient values are observed at the eastern side of the area. It is observed that, the pattern of high gradient anomalies is broad, not like sharp ones of the ideal vertical boundaries of sharp density contrast. One explanation of this pattern is that, the boundaries in the area are not completely vertical and relatively deep and/or the anomalies are produced by several boundaries. Grauch and Cordell (1987) discussed the limitations of the horizontal gradient method for gravity data and concluded that, the horizontal gradient magnitude maxima can be offset from a position directly over the boundaries if the boundaries, are not near-vertical and close to each other. Figure (5) shows, also, a tentative qualitative interpretation of the produced horizontal gradient data. Generally, the area may be dissected by major boundaries striking in the NE-SW, with NW-SE trend that does show up towards the western side of the study area.

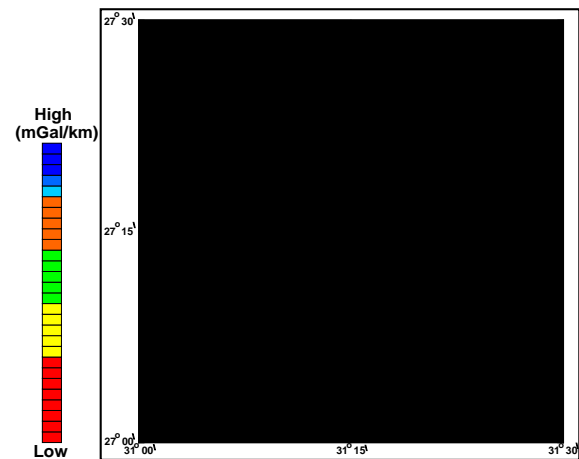


Figure 5: Horizontal gradient map of the Bouguer gravity data. The dashed lines indicate the locations of the deduced faulting elements.

2) Analytical Signal Method:

The analytical signal method is known as the total gradient method, and as defined here, it produces a particular type of calculated gravity or magnetic anomaly enhancement map used for defining, *in a map sense*, the edges (boundaries) of geologically anomalous density or magnetization distributions. In exploration potential field applications, the term analytical signal loosely refers to the calculated modulus of the gravity or magnetic anomaly field's three mutually- orthogonal spatial (X, Y, and, Z) derivative terms. Analytical signal maxima have the useful property that, they occur directly over faults and contacts, regardless of the structural dip which may be present, and independent of the direction of the induced and/or remnant body

magnetizations (in case, if it is applied to magnetic data). Mapped maxima (ridges and peaks) in the calculated analytical signal of a gravity or a magnetic anomaly map locate the anomalous source body edges and corners (e.g., basement fault block boundaries, basement lithology contacts, fault/shear zones, igneous and salt diapirs,... etc.).

The basic concepts of the analytical signal method in the two-dimensional magnetic data were extensively discussed by Nabighian (1972, 1974 and 1984). Their counterparts, in the case of gravity data, have been introduced by Klingele *et al.* (1991). Marson and Klingele (1993) defined the analytical signal of the vertical gravity gradient produced by a three-dimensional source as follows:

$$|A_g(x, y)| = \sqrt{\left(\frac{\partial g}{\partial x}\right)^2 + \left(\frac{\partial g}{\partial y}\right)^2 + \left(\frac{\partial g}{\partial z}\right)^2} \quad (2)$$

where: $|Ag(x, y)|$ is the amplitude of the analytical signal at (x, y) , g is the observed gravity field at (x, y) , and $\frac{\partial g}{\partial x}$, $\frac{\partial g}{\partial y}$ and $\frac{\partial g}{\partial z}$ are the two horizontal and vertical derivatives of the gravity field, respectively.

The unusual feature of this technique is its use for interpreting the gravity data. Hansen *et al.* (1987) suggested that the straight-forward application of Poisson's relation (Baranov, 1957) and the correspondence between gravity and magnetic fields for homogeneous bodies would suggest the use of analytical signal of the vertical gradient of gravity data. This relates the vertical gradient of gravity data from a given source to the magnetic effect of the same source. Starting from this consideration, one can apply magnetic interpretation methods to gravity data. Klingele *et al.* (1991) showed in their paper that, the analytical signal could be applied directly to airborne gravity gradiometric data, as well as the ground gravity surveys after transformation of the Bouguer anomalies into vertical gradient anomalies.

Stanley and Green (1976) stated that, "gravity gradient information are more sensitive to geological structures than gravity itself, and gradient interpretation is less susceptible to the interference from neighboring structures". The application of the analytical signal method to gravity data was first suggested by Nabighian (1972), but he did not apply this concept to gravity data really.

The analytical signal is peaked over the location of the top of the contact. For geologic models, the shape of the analytical signal is a bell-shaped symmetrical function located above the source body. In addition, depths can be obtained from the shape of the analytical signal (MacLeod *et al.*, 1993). Figure (6) illustrates the distribution of the analytical response in the study area with the direction of profiles used to estimate the depths to the tops of faults.

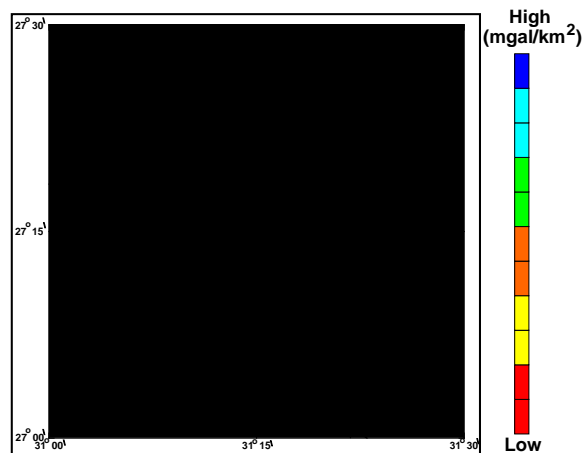


Figure 6: Analytic signal of the Bouguer gravity data. Lines 1-12 are the selected profiles that were used to estimate the depths.

3) Depth estimation from the Analytical Signal Method:

The analytical signal anomaly over a 2-D gravity (or magnetic) contact located at x and at depth h is described by the expression (after Nabighian, 1972):

$$|A(x)| = \alpha \cdot \frac{1}{(h^2 + x^2)^{1/2}} \quad (3)$$

where: $|A(x)|$ is the analytical signal, and (α) is the amplitude factor. The analytical signal described by equation (3) is a simple bell-shaped function (as shown in Figure 7).

The shape of the analytical signal is dependent only on depth. For a contact, taking the second vertical derivative of Equation (3) with respect to (x) produces the following results:

$$\frac{d^2 |A(x)|}{dx^2} = \alpha \cdot \frac{2x^2 - h^2}{(h^2 + x^2)^{5/2}} \quad (4)$$

After re-arranging Equation (4),

$$\text{we obtain } x_i = 2^{1/2} \cdot h = h \cdot \sqrt{2} \quad (5)$$

where: h is the depth to the top of contact and x_i is the width of the anomaly between minima points.

To estimate the depth to the contacts from the analytical signal method, twelve profiles were selected, where the anomalous high analytical signal responses due to significant density contrasts (that produced such identifiable signatures) found on the map. Equation (5) was used to calculate the depth for each profile to the top of its corresponding contact. The delineated fault/contact pattern is shown in Fig. 8 and the estimated depths to such contacts are shown in Table 1.

Table (1) shows the depth values to the tops of interpreted faults/contacts (Fig.6)

Profile No.	Depth to top of the fault (km)	Profile No.	Depth to top of the fault (km)
1	5.23259	7	4.879037
2	5.020458	8	4.808326
3	5.23259	9	4.949747
4	4.949747	10	5.197235
5	4.949747	11	5.020458
6	4.879037	12	5.868986

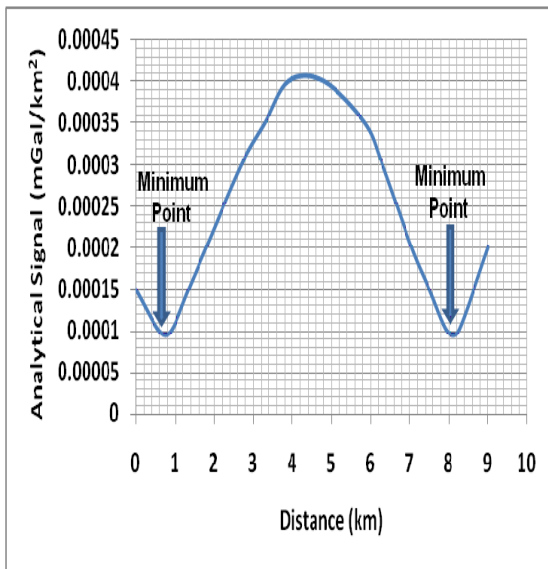


Figure 7: Amplitude of the analytic signal of profile 12

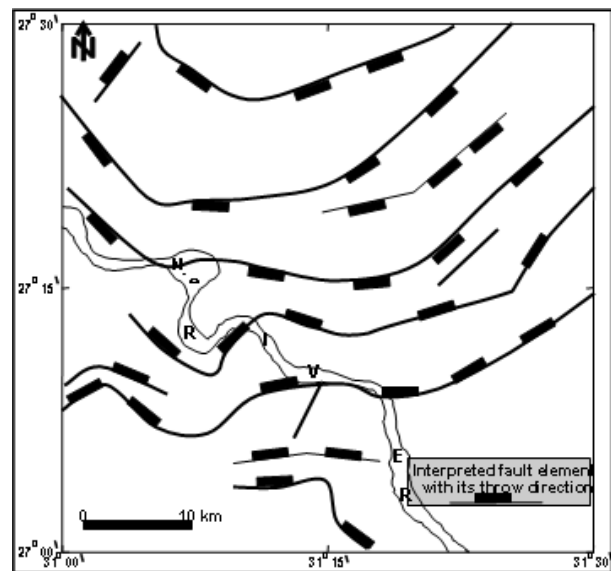


Figure 8: Map showing the interpreted fault pattern from Analytical Signal Response

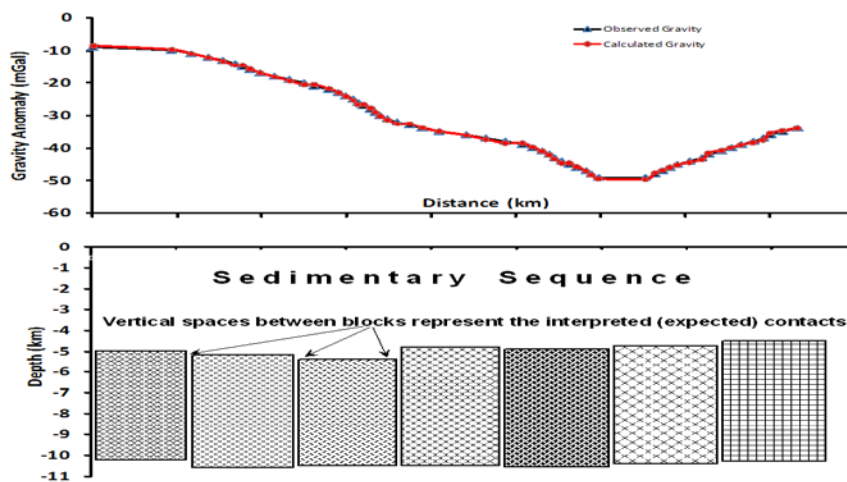


Figure 9: Conceptual model for the basement configuration in the along the profile A1-A2.

SUMMARY AND CONCLUSIONS

Through this work, the Bouguer gravity map of Wadi El-Assuity area has been used to detect the subsurface structural features in the study area. First, the horizontal gradient technique was applied to the Bouguer gravity anomaly map. The horizontal gradient results of the gravity map exhibited the general expected structural trends in the area under study.

These are represented by a number of expected fault elements of a general NE-SW trend in the eastern half of the study area, where Wadi El-Assuity exists. The NW trending faults are observed in the Nile Valley in the west and southwest of the study area. Applying the analytical signal technique was more resolving for the expected deep structural elements. Depths to the tops for some of the expected deep faulting elements were calculated. Analytical signal gravity map showed that, the northeastern gravity gradient of the Bouguer anomaly map can be interpreted as being represented by a number of parallel fault elements of slightly different depths, but with almost two fault trends. Other fault elements were also detected around the Nile River area. The interpreted fault pattern exhibited these faulting trends through the application of the analytical signal technique.

Youssef et al (1998), through their study within Sohag area (to the south of the current study area) mentioned that, their estimated depths to the basement surface in their area reached about 4 kilometers, with some uplifted and downfaulted basement blocks through some fault elements oriented east-northeast, northwest, and east-west.

The interpreted fault pattern in the present study area shows more east-northeast to northeast oriented fault trend with somehow deeper fault elements. Less prominent NW trending faults are detected to the west of the study area that is connected with the other fault trends. That is acceptable, since the depths to basement surface in Egypt generally increase northwardly. Since the depths to interpreted faults are close to each other, so it is expected that the surface Bouguer gravity variations are attributed to the lateral variation in density within the basement rocks. Therefore, a conceptual subsurface model for the basement configuration in the study area has been constructed along the direction A1-A2 (Figure 3) to manifest the lithologic variations within the basement rocks. The author used variable density contrast values ranging from 0.2 to 0.35 gm/cc. Higher density contrasts were towards the flanks of the profile, while smaller density contrasts were towards the central part of the profile. So, it is expected that the basement lithologic composition is not too different within the central part of the profile, while shows gradual and faster variation towards both ends of the profile. From the concluded remarks, it can be deduced that the basement lithologic variations include both intra-basement and supra-

basement features. The idea about expected supra-basement features emerges from the resulted differences of depths to the contacts (boundaries) of the basement. While, the expected intra-basement occurrences emerge from varying density contrasts that have been used in constructing the general conceptual model shown in Figure (9).

These variations in depths to some studied contacts (shown in Fig. 9) should have their impact on the overlying sedimentary sequence. Consequently, small scale structural features within the sedimentary section may exist in the form of minor synclines and anticlines or a number of uplifted and down-faulted strata. Mapping such probable structural features within the sedimentary sequence is not included in the scope of the present work.

Some mapable faulting features can be deduced from the Bouguer anomaly map (Fig.3), but are not involved in the mapped contacts/boundaries (Fig.8). This is probably due to the fact that, the mapped contacts in Figure (9) are deep rooted (as concluded from the application of the analytical signal) within the basement, while the non included mapable faulting may originate within the sedimentary sequence. That is why; such sedimentary offsets were not shown in the faulting pattern deduced from the analytical signal approach. on Figure (9). The faults affecting the study area have NE trend inside Wadi El-Assuity in the east and NW trend toward the Nile Valley in the west and southwest. The NE oriented fault bounding the southeastern side of El-Assuity coalesces with a zigzag fault system that extends to the Western Desert. The faults form a NE elongated graben in Wadi El-Assuity that changes its trend to have NW trend inside the Nile Valley.

REFERENCES

- Abd-Allah, A.M.A., 2008:** Structural evolution of the intracontinental Nile Valley rift, Egypt. *Journal of Applied Geophysics*, Volume, 7, Number 1, 49-75.
- Abdel-Monem S.M., Sakr K., Hassoup A., Mahmoud S., Tealeb A., Al-Ibiary M. and Mansour M.; (2004):** Crustal deformation measurements and seismicity of the middle part of the Nile Valley in Egypt. *Egyptian Geophysical Society. EGS Journal*, vol. 2, No. 1, 123-133 (2004)
- Attia M.M.; (1995):** Geological and geophysical studies on the sedimentary basin at Sohag area. Ph.D.Thesis, South Valley Univ. Geology. Dept., Fac. Sci. (Sohag).
- Bakheit A.A.; (1989):** Geological and geophysical studies on the areas around Wadi El Assiuty. Eastern Desert Egypt. Ph.D. Thesis, Assiut University.

- Baranov V. (1957):** A New method for interpretation of aeromagnetic maps: Pseudo-gravimetric anomalies. *Geophysics*, 22(1957), pp. 359-383.
- Blakely R.J.; (1995):** Potential theory in gravity and magnetic applications. Cambridge Univ. Press, 1995.
- Blakely, R.J. and Simpson, R.W.; (1986):** Approximating edges of source bodies from magnetic or gravity anomalies. *Geophysics* 51, 1494 - 1498.
- Cooper, G.R.J., and D.R. Cowan, 2003,** Sunshading geophysical data using fractional order horizontal gradients. *The Leading Edge*, 22, 204.
- Cordell L. and Grauch V.J.S.; (1985):** Mapping basement magnetization zones from aeromagnetic data in the San Juan Basin. New Mexico, in Hinze, W.J., Ed., *The utility of regional gravity and magnetic anomaly maps: Sot. Explor. Geophys.*, 181-197.
- Cordell, L.; (1979):** Gravimetric expression of graben faulting in Santa Fe Country and the Espanola Basin, New Mexico. *New Mexico. Geol. Sot. Guidebook*, 30th Field Conf., 59-64.
- Eaton, D., and K. Vasudevan, 2004,** Skeletonization of aeromagnetic data. *Geophysics*, 69, 478-488.
- Grauch V.J.S. and Cordell L.; (1987):** Short note, Limitations of determining density or magnetic boundaries from the horizontal gradient of gravity or pseudogravity data. *Geophysics*, 52, 118-121.
- Hansen, R. O., R.S. Pawlowski, and X. Wang, (1987):** Joint use of analytic signal and amplitude of horizontal gradient maxima for three-dimensional gravity data interpretation, 57th SEG meeting, New Orleans, extended Abstracts, pp. 100-102, 1987.
- Kenan Gelisli and Nafiz Maden; (2006):** Analysis of potential field anomalies in Pasinler-Horasan basin, Eastern Turkey. *Journal of the Balkan Geophysical Society*, Vol. 9, No. 1, December 2006, p. 1-7, 6 figs.
- Klinge, E.E., and Marson, I., (1991):** Automatic interpretation of gravity gradient data in two dimension: Vertical gradient. *Geophys. Prospect.*, 39, 407-439.
- MacLeod, I.N., K. Jones, and T.F. Dai, (1993):** 3-D analytic signal in the interpretation of total magnetic field data at low magnetic latitudes, *Exploration Geophysics*, 679-688, 1993.
- Marson, I., and Klinge, E.E., (1993):** Advantages of using the vertical gradient of gravity for 3-D interpretation. *Geophysics*, 58, 1588-1595.
- Nabighian M.N., Ander M.E., Grauch V.J.S., Hansen R.O., LaFehr T.R., Li Y., Pearson W.C., Peirce J.W., Phillips J.D., and Ruder M.E.; (2005):** Historical development of the gravity method in exploration.
- Nabighian M.N.; (1972):** The analytic signal of two-dimensional magnetic bodies with polygonal cross-section: Its properties and use for automated anomaly interpretation. *Geophysics*, 37, 507-517.
- Nabighian M.N.; (1974):** Additional comments on the analytic signal of two-dimensional magnetic bodies with polygonal cross-section. *Geophysics*, 39, 85-92.
- Nabighian M.N.; (1984):** Toward the three dimensional automatic interpretation of potential field data via generalized Hilbert transforms: Fundamental relations. *Geophysics*, 53, 957-966.
- Omara S. and El-Tahlawi M.R.; (1972):** Limestone "dykes" in the Nile Valley around Assiut, Upper Egypt. *N.Jb. Geol. Palaont. Mh. Jg.*, H.8, pp. 475-483.
- Pearson W.C.; (2001):** Aeromagnetic imaging of fractures in a basin centered gas play. *AAPG Explorer*, 22, no. 5, 52-55.
- Phillips J.D.; (1998):** Processing and Interpretation of Aeromagnetic Data for the Santa Cruz Basin-Patahonia Mountains Area, South-Central Arizona. U.S. Geological Survey Open-File Report 02-98.
- Roest, W. R., J. Verhoef, and M. Pilkington, 1992,** Magnetic interpretation using the 3D analytic signal. *Geophysics*, 57, 116-125.
- Said R.; (1962):** The geology of Egypt. Elsevier, Amsterdam, 377pp.
- Said R.; (1981):** The Geological Evolution of the River Nile. Springer, 151 pp.
- Said R.; (1992):** The Geology of Egypt. Elsevier Science Ltd., Rotterdam, Netherlands.
- Stanley J.M. and Green R.; (1976):** Gravity gradients and the interpretation of the truncated late. *Geophysics*, 41, 1370-1376.
- Stern R.J., Gottfried D., Hedge C.E.; (1984):** Late Precambrian rifting and crustal evolution in the Northeastern Desert of Egypt. *Geology* 12, 168-172.
- Stern R.T. and C.E. Hedge; (1985):** Geochronologic and isotopic constrains on Late Precambrian crustal evaluation in the Eastern Desert of Egypt. *Am. J. Sci.*, 285, 97-127, 1985.
- Thurston, J. B., and R. J. Brown, 1994,** Automated source-edge location with a new variable-pass horizontal gradient operator. *Geophysics*, 59, 546-554.
- Youssef M. M., Ibrahim H. A., Bakheit A. A. and Senosy M. M.; (1994):** Surface and subsurface tectonic pattern of Sohag region, Middle Egypt. *Bull. Fac. Sci., Assiut. Univ.*, Vol. 23, No. (1-F), pp. 317- 360.

SOIL/BEDROCK CHARACTERISATION AND ENGINEERING PARAMETERS CALCULATIONS FOR THE KANTO REGION, CENTRAL JAPAN

M.M.F. Shokry⁽¹⁾ and N. Hirata⁽²⁾

1- Department of Geophysics, Faculty of Science, Ain Shams University, Cairo, Egypt, 11566
2- Earthquake Prediction Research Centre, Earthquake Research Institute, Tokyo University, Japan

خصائص التربة/الصخر الأساس وحساب المعاملات الهندسية لمنطقة الكانتو، بوسط اليابان.

الخلاصة: تم استخدام المعلومات المتاحة والخاصة بشبكتي رصد الزلازل (*K-NET and KiK-net*) وذلك من أجل عمل تقييم إقليمي لمنطقة الكانتو. ومن خلال هذه الدراسة تم عمل تقييم لمنطقة الدراسة من خلال دراسة الخصائص الهندسية والجيوتقنية لكل من طبقات التربة وصخر الأساس وذلك لخدمة الأهداف الهندسية. حيث تم حساب عدد من المعاملات الهندسية مثل معامل التركيز، معامل المادة، معدل تدرج الكثافة ونسبة التضغط، وذلك من خلال الاستعانة بالمعلومات المتاحة والخاصة بشبكتي رصد الزلازل (*K-NET and KiK-net*) بالإضافة إلى أنه تم الاستعانة أيضا بعدد من تسجيلات الآبار الضحلة والعميقة والتي تصل إلى صخور القاعدة في بعض الآبار. ولقد أظهرت نتائج المعاملات الهندسية التي تم حسابها والتي شملت قيم السرعات السيزمية ومعاملات الإنضغاط الهندسية توافيقها مع النظام التركيبي الرسوبي السائد والمميز لمنطقة الكانتو. وأظهرت أيضا هذه الدراسة أهمية الاستفادة من المعلومات المتاحة والخاصة بشبكتي رصد الزلازل (*K-NET and KiK-net*) على موقع الإنترنت.

ABSTRACT: Data from *K-NET* and *KiK-net* were used to evaluate regional site effects in the Kanto region. The present study delineates some of the shallow soil/bedrock engineering characteristics for construction purposes. A number of engineering parameters, such as Concentration Index C_i , Material Index γ , Density Gradient D_i and Stress Ratio S_i , were estimated using *K-* and *KiK-NETS* data together with shallow/deep borehole recordings obtained from the pre-Tertiary basement. Estimated parameters, which include seismic velocity values, engineering, consolidation and strength parameters showed that, these parameters are strongly correlated with the structure of the sedimentary layer-bedrock system in the Kanto region. The present study also delineates the usefulness of the *K-NET* and *KiK-net* data, which are now available on the internet site (www.k-net.bosai.go.jp/).

INTRODUCTION

The Kanto region of Central Japan, which includes Tokyo, is located on Honshu, the largest island in Japan. The Kanto region is the centre of political and economic activities in Japan, and also contains one third of Japan's population. Its boundary is nearly the same as that of the Kanto plain. The region consists of seven prefectures: Gunma, Tochigi, Ibaraki, Saitama, Tokyo, Chiba and Kanagawa. It is one of the most active seismic zones in the world, and many disastrous earthquakes have occurred in and around the region. Due to the complex relative movement of the Philippine Sea, Pacific and the North American plates, complicated tectonic structures exist in this region, and several types of earthquake mechanisms have been observed (Okada and Kasahara, 1990; and Ishida, 1992). Recently, the metropolitan area has seen a large increase in the number of large-scale buildings, such as tall skyscrapers and large oil and gas tanks. The natural periods of these structures are long; thus they would be expected to respond to long-period ground motions determined by the sedimentary basin structure and the geophysical properties of bedrocks, basement rocks and sediments. More than 3000-meter thick sediments lie on the pre-Tertiary basement (the sedimentary section-basement system) beneath the Kanto region, similar in structure to many metropolitan areas throughout the world. Previous interpretations, based on geophysical exploration,

suggest that the shape of the base of this sedimentary basin is smooth (Komazawa and Hasegawa, 1988; Koketsu and Higashi, 1992; Yamanaka and Yamada, 2002; and Suzuki, 2002) (Fig. 1).

Accurate evaluation of ground amplification characteristics requires detailed soil profile information, such as shear-wave velocity structures. It has been pointed out, however that, approximate estimation of ground amplification is possible with the shear-wave velocity of the surface layer (Borcherdt and Gibss, 1976) and that, the amplification of strong ground motion, such as peak ground velocity is correlated with the average shear-wave velocity from the surface to a certain depth (Joyner and Fumal, 1984; Midorikawa et al., 1994).

The ultimate goal of the present study is to recommend soil/bedrock characterisation and engineering parameters calculations for the Kanto region, based on the measured and calculated shallow engineering characteristics. Analysis of the down-hole seismic velocities (P-wave and S-wave) and density values could tangibly delineate the soil/bedrock layering

in the study area, and also determine the following soil/bedrock engineering parameters: Poisson's Ratio, Young's Modulus, Lamé's Constants, Concentration Index, Material Index, Density Gradient and Stress Ratio.

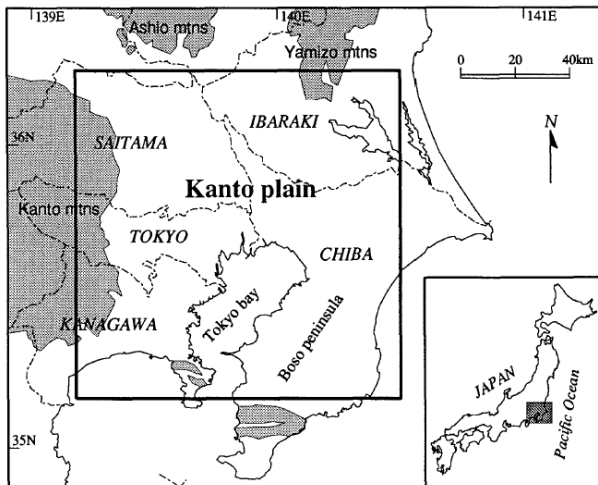


Fig. (1): Index map showing the location of the Kanto Region and its geographical and geological setting. The pre-Tertiary basement outcrops are shown in the shaded areas. The rectangle drawn with thick lines indicates the 120 × 120 km target area of the Kanto Region. The capital letters in italics designate the names of the prefectures in the Kanto Region.

To implement the engineering parameters calculations, data from systematic networks of strong-motion observation are needed. The National Research Institute for Earth Science and Disaster Prevention (NIED) constructed a strong-motion network, the K-NET (Kinoshita, 1998), followed by the construction of a high sensitivity digital strong-motion seismograph network (KiK-net) across all of Japan. The data from the K-NET and KiK-net are now available on the internet. In the present study, soil conditions information for the Kanto region were determined using K-NET and KiK-net sites data released on the internet.

DATA

The boundary between soil and bedrock is rarely distinct. It is usually gradual, making up a transition zone instead of a clear-cut interface. Residual soil (rock weathered or decomposed into a soil layer *in-situ*) is often encountered. When a residual soil layer is present in the transition zone, gravel, cobblestones and boulders may also exist, obscuring the location of the soil boundary. Below are few definitions of soil and rock taken from dictionaries of varying disciplines. The dictionary of Geological Definitions (Kulhawey et al., 1991) defines the term 'soil' as equivalent to regolith and 'bedrock' as any solid rock exposed at the surface of the earth or overlain by unconsolidated material. However, the Penguin Dictionary of Civil Engineering (Kulhawey et al., 1991) defines 'soil' as "gravels, sands, silts, clays, peat and all other loose materials including topsoil down to bedrock", and 'bedrock' as "rock underlying gravel or other loose surface soil". The representative values for shear-wave velocity possess

through the following material classification limits: soft soil (less than 600 m/sec), firm soil (between 600 and 1800 m/sec), and rock (greater than 1800 m/sec) (Sjogren *et al.*, 1979). The last classification, the definition of which depends on the shear-wave velocity values, was used in the present study to differentiate between the sedimentary cover and the bedrock.

We used the down-hole soil conditions information from the K-NET and KiK-net station sites, which are well distributed in the Kanto region with a station-to-station distance of about 25 km. K-NET site data contain shallow down-hole soil conditions information (P-wave and S-wave velocities, as well as density values) for 110 stations. The down-hole measurements were obtained between depths of 10 to 20 m. At 33 stations, the borehole logs record the bedrock at various depths below the soil layer (sedimentary cover), but at the other 77 stations, bedrock is not recorded until the end of the borehole logs, while the sedimentary layer extends to the end depth of the borehole. However, KiK-net sites data contain deep down-hole soil measurements (P-wave and S-wave velocities) between about 100 to 2000 m in depth for 58 stations, that are well distributed in the Kanto region (Fig. 2).

ENGINEERING PARAMETERS

Elastic properties of the near-surface materials and their effects on seismic wave propagation are very important in earthquake and civil engineering, as well as in environmental and earth science studies. The increased amplitudes of soft sediments are one of the most important factors responsible for the amplification of earthquake motions. Amplification is proportional

$$\frac{1}{\sqrt{V_s \cdot \rho}} \quad (1)$$

where: (V_s) is the shear-wave velocity and (ρ) is the density of the investigated soil (Aki & Richards, 1980). No construction material has more variable engineering and physical parameters than the ground's soil. These parameters vary both laterally and vertically, and the variations are often robust (Bowles, 1982). In order to evaluate the competence of the subsurface for construction, some of the shallow soil engineering parameters were calculated. Four parameters were calculated; the Concentration Index (C_i), the Material Index (γ), the Density Gradient (D_i), and the Stress Ratio (S_i). Integration of these four parameters was used to classify the most appropriate areas of the Kanto region for construction.

Two types of units encountered in the Kanto region, identified on each lithologic column of the borehole logs and used from the K-NET and KiK-net sites, were the soil unit (sedimentary cover) and the bedrock unit. In order to calculate the above-mentioned parameters, the values of weighted mean values for V_p ,

V_s and density (ρ) for the sedimentary cover and the bedrock were computed using the following formula:

$$V_p = \frac{\sum_{i=1}^n h_i}{\sum_{i=1}^n \frac{h_i}{V_{pi}}} \quad (2)$$

where: (h_i) and (V_{pi}) denote the thickness (in m) and the compressional wave velocity (in m/s) of the i -th layer in a total of n layers present in the same type of unit (Eurocode, 2001 and Romanian code, 2006). P and

S -wave velocities and density were obtained from the acquired P - S logging data. When density data were lacking in some P - S logs, the following models relating density (in units of gm/c.c) and P -wave velocity (in km/sec) were applied: when $V_p < 1.5$ km/sec: $\rho = 1.93$ gm/cm³ (Boore, 2007); if 1.5 km/sec $\leq V_p < 6.0$ km/sec, then $\rho = 1.74V_p^{0.25}$ (Gardner et al., 1974). Poisson's Ratio (σ), Young's Modulus (E), Lamé's Constant (λ) and the Shear Modulus (μ) were also required. These elastic moduli values were calculated from the equations listed in Table 1.

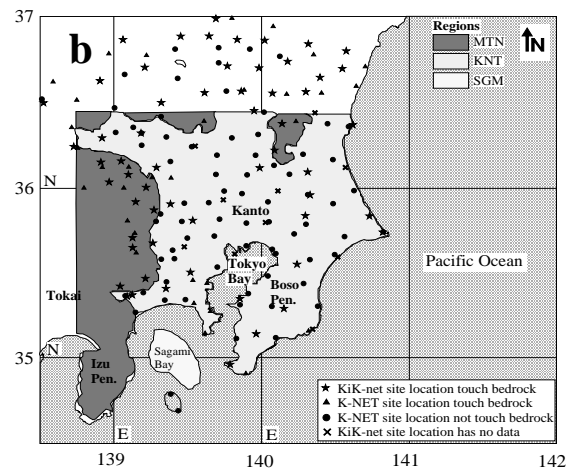


Fig. (2): a: Regional topographic map of Japan showing the finite difference (FD) grid area (black rectangle) of the Kanto district, including the Tokyo metropolitan area. Seafloor topography around Japan is also shown (Smith and Sandwell, 1997). b: Map showing the whole FD grid area and stations included in this study. Stars, triangles, circles, and crosses indicate the KiK-net site locations that reached bedrock, the K-NET site locations that reached bedrock, the K-NET site locations that did not reach bedrock, and the KiK-net site locations lacking data, respectively. The regions displayed in dark, medium, and light grey are the mountain region (MTN), the Kanto basin region (KNT), and the Sagami basin region (SGM) along the Sagami Trough, respectively. c: Geological map of the area surrounding the Kanto region reproduced from the Geological Survey of Japan (1992).

Table 1: List of equations used to calculate elastic moduli

Elastic Modulus	Equation used	Reference
Poisson's Ratio	$\sigma = \frac{1}{2} \left[1 - \frac{1}{(V_p/V_s)^2 - 1} \right]$	Adams (1951) and Salem (1990)
Young's Modulus	$E = \rho \frac{3V_p^2 - 4V_s^2}{(V_p/V_s)^2 - 1}$	Adams (1951)
Lame's Constants	$\lambda = \frac{\sigma E}{(1 + \sigma)(1 - 2\sigma)}$	King (1966) and Toksoz et al. (1976)
Shear Modulus	$\mu = \frac{E}{2(1 + \sigma)}$	King (1966) and Toksoz et al. (1976)
Elastic Modulus	Equation used	Reference
Poisson's Ratio	$\sigma = \frac{1}{2} \left[1 - \frac{1}{(V_p/V_s)^2 - 1} \right]$	Adams (1951) and Salem (1990)
Young's Modulus	$E = \rho \frac{3V_p^2 - 4V_s^2}{(V_p/V_s)^2 - 1}$	Adams (1951)
Lame's Constants	$\lambda = \frac{\sigma E}{(1 + \sigma)(1 - 2\sigma)}$	King (1966) and Toksoz et al. (1976)
Shear Modulus	$\mu = \frac{E}{2(1 + \sigma)}$	King (1966) and Toksoz et al. (1976)

V_p and V_s are the P- and S-wave velocities, respectively.

The elastic moduli results for the bedrock unit can be summarised as follows:

1. Soil cover thickness (depth to bedrock) ranged from 0.0 m (bedrock cropped out on the surface at station TKY002) to 250 m. Compared with the mountainous region (MTN) to the north and west, the central part of the Kanto basin region (KNT) is characterised by relatively thick soil cover (Fig. 3a). 2. Compressional wave velocity (V_p) is ranged from 650 to 4700 m/sec (Fig. 3b). 3. Shear wave velocity (V_s) is ranged from 255 to 2100 m/sec. The central part of the study area in the KNT region is characterised by relatively low shear-wave velocity values; these values increase toward the MTN region (Fig. 3c). Based on the shear-wave velocity, the bedrock is classified as firm soil (Sjogren *et al.*, 1979) in most parts of the study area, except in the KNT region, where it is classified as soft soil due to the low shear velocity values recorded.

However, the geological description of the samples on the borehole logs refers to bedrock identification (Fig. 3d). 4. Bulk density (ρ) is ranged from 1.53 to 2.57 gm/cc. The area towards the northeast is characterised by relatively high rock densities. 5. Poisson's ratio (σ) is ranged from 0.083 to 0.495. 6. Young's modulus (E) is ranged from 333 to 31174 MPa (Mega Pascal = (Newton/m²)/10⁶). 7. Lame's constant (λ) is ranged from 160 to 34104 MPa. 8. Shear modulus (μ) or Rigidity modulus is ranged from 112 to 11334 MPa.

The northwestern and western parts of the area are characterised by relatively low Poisson's ratio values, indicating more competent soil in this part of the study area (Salem, 1990). The eastern part is characterised by relatively high values for Young's modulus, relatively low (λ) values, and relatively high rigidity or shear modulus (μ) values.

The elastic moduli results for the soil cover can be summarised as follows:

1. Compressional wave velocity (V_p) is ranged from 200 to 1900 m/sec (Fig. 4a). 2. Shear wave velocity (V_s) is ranged from 100 to 700 m/sec (Fig. 4b). The soil cover over the Kanto region is classified as soft soil, according to the shear-wave velocity (Sjogren *et al.*, 1979), excluding two sites (GNM015 and TCGH17), where the soil cover is classified as firm soil. 3. Bulk density (ρ) is ranged from 1.35 to 2.09 gm/cc (Fig. 4c). The area towards the central portion of KNT is characterised by relatively high soil densities. 4. Poisson's ratio (σ) is ranged from 0.24 to 0.5. 5. Young's modulus (E) is ranged from 43 to 2622 MPa. 6. Lame's constant (λ) is ranged from 39 to 6577 MPa. 7. Shear modulus (μ) or Rigidity modulus is ranged from 14 to 956 MPa.

The northwestern and western parts of the area are characterised by a relatively low Poisson's ratio, indicating more competent soil in this part of the study area. The central portion of KNT is characterised by relatively high values for Young's modulus, (E) values, and rigidity or shear modulus (μ) values.

At frequencies that approach the fundamental frequency (f_o) of the soil deposit, the transfer function began to take on large values. However, at frequencies above the fundamental frequency, a part of the soil deposits may be moving in one direction, while another part is moving in the opposite direction. The period of vibration corresponding to the fundamental frequency is termed the characteristic site period (T_s). T_s provides a very useful indication of the period of vibration, at which the most significant amplification can be expected. f_o and T_s were computed by using the following formulas: $f_o = (V_s/4H)$ and $T_s = (4H/V_s)$, respectively, where (V_s) is the shear-wave velocity and (H) is the soil cover thickness (Kramer, 2004). f_o is ranged from 0.38 to 32.5 Hz (Fig. 5a). T_s is ranged from 0.03 to 2.62 sec (Fig. 5b).

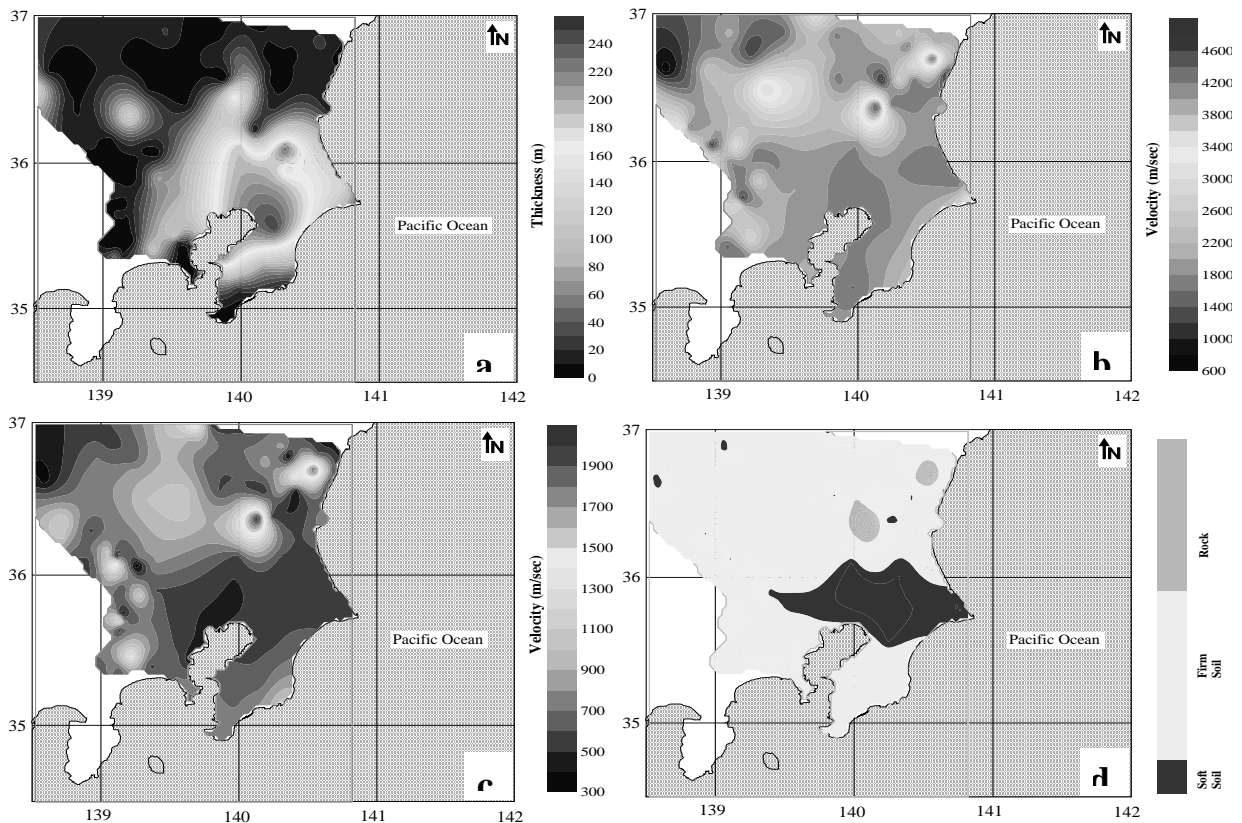


Fig. (3): a: Contour map illustrating the depth to the bedrock (sedimentary cover thickness). b: Contour map illustrating the compressional (P) wave velocity of the bedrock. c: Contour map illustrates the shear (s) wave velocity of the bedrock. d: Contour map illustrates the shear (s) wave velocity classification of the bedrock.

The area towards the central portion of KNT was characterised by relatively low $f_{o,}$, which decreased as the soil cover thickness increased (Fig. 5c), but by relatively high T_s , corresponding to thick soil cover thickness with a nearly linear relationship (Fig. 5d). The results are consistent with those of Kinoshita and Ogue (2002), who found that high site amplification zones at low frequency bands of 0.5 and 1.0 Hz correspond to zones, in which the thickness of the soil layer exceeds 2.0 km, i.e., where the site amplification becomes large proportional to the thickness of the soil layer. At high frequency bands of 8 and 16 Hz, high site amplification zones correspond to mountainous areas; the Kanto mountains and high site amplification areas move from thick sediment zones to mountainous areas at frequency bands of 2.0 and 4.0 Hz.

Using the seismic velocities and elastic moduli values, the shallow soil/bedrock engineering parameters were calculated. These parameters include the Concentration Index, the Material Index, the Density Gradient, and the Stress Ratio.

The Concentration Index (C_i)

The Concentration Index is an engineering parameter, that indicates the degree of material

concentration or impaction (competence) for foundation and other civil engineering purposes. It depends mainly on the elastic moduli of the materials and the depth-pressure distribution. Therefore, C_i is a material-dependent factor. Bowles (1982) formulated the concentration index in terms of Poisson's ratio (σ) as:

$$C_i = \frac{(1 + \sigma)}{\sigma} \quad (3)$$

Abd El-Rahman (1991) measured C_i in terms of velocities (P- and S-wave velocities, V_p and V_s) as:

$$C_i = \left(3 - 4 \left\{ \frac{V_s^2}{V_p^2} \right\} \right) / \left(1 - 2 \left\{ \frac{V_s^2}{V_p^2} \right\} \right) \quad (4)$$

Abd El-Rahman (1989) summarised the ranges of the concentration index (C_i) corresponding to the degree of soil competence (Table 2). In the study area, the calculated (C_i) for the bedrock layer revealed values ranging from 3.02 to 12.99 (Fig. 6a). The northwestern part is characterised by relatively high (C_i) values, which according to Abd El-Rahman (1989), reflect fairly competent soft to good competent soil (Fig. 6b). For the soil cover, the calculated (C_i) displayed values ranging from 3.02 to 5.23 (Fig. 6c).

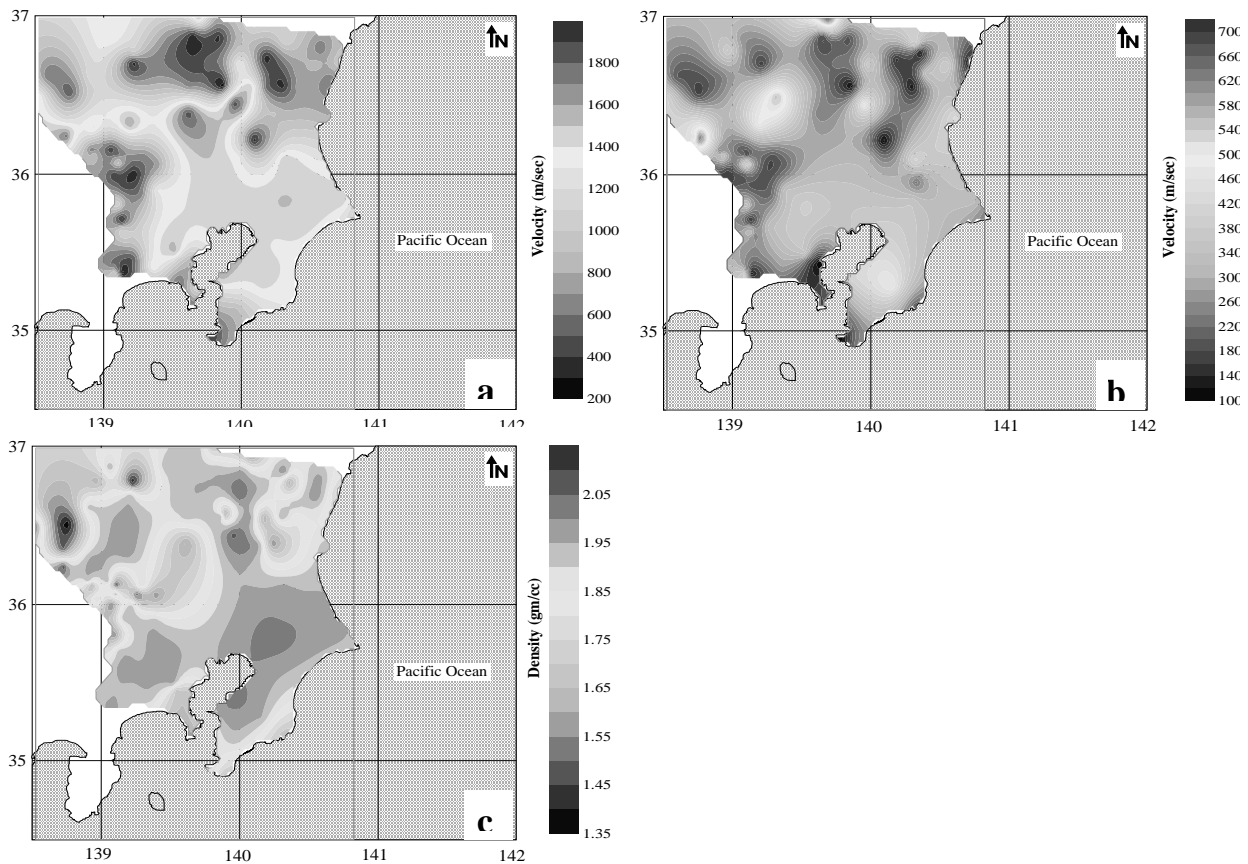


Fig. (4): a: Contour map illustrating the compressional (P) wave velocity of the sedimentary cover. b: Contour map illustrating the shear (s)-wave velocity of the sedimentary cover. c: Contour map illustrating the bulk density of the sedimentary cover. d: Gravity anomaly map reproduced from Kono and Furuse (1989). This anomaly map, includes the gravitational effects of subducting Philippine and Pacific slabs. The contour interval is 20 mgal.

The Kanto basin is characterised by relatively low (C_i) values, which classify this region as comprising non-competent, very soft soils to non-competent, soft soils toward the north-northwestern parts (Fig. 6d).

The Material Index (γ)

From the engineering viewpoint, the material index parameter defines the material quality for foundation purposes. According to Abd El-Rahman (1989), this expression addresses the degree of competence based on the elastic moduli of the given material. Thus, this index is associated with the composition of the material, the degree of consolidation, fracturing, jointing and the presence or absence of fluids in the pore space, all of which affect the medium of the materials and, consequently the wave velocities. Abd El-Rahman (1989) derived the material index from the ratio between Lamé's constant (λ) and the rigidity modulus (μ) or in terms of Poisson's ratio (σ) as follows:

$$\gamma = \frac{(\mu - \lambda)}{(\mu + \lambda)} = (1 - 4\sigma) \quad (5)$$

According to Birch (1966), Gassman (1973), Tatham (1982) and Sheriff and Geldart (1986), Table 3 shows the Poisson's ratio, rigidity modulus and material index corresponding to various materials. For construction purposes, the soil properties can be classified by the material index into four main categories (Table 4). In the study area, the calculated material index (γ) for the bedrock layer revealed values ranging from -0.98 to 0.67 (Fig. 7a). The northwestern part was characterised by relatively high (γ) values, reflecting fairly to moderately competent material (Fig. 7b). For the soil cover, the calculated (γ) displayed values ranging from -0.98 to 0.06 (Fig. 7c). The Kanto basin is characterised by relatively low material index (γ) values, which are classified as non- to less-competent materials, but towards the north-northwestern parts, the material indices suggested that, the soils are fairly to moderately competent (Fig. 7d).

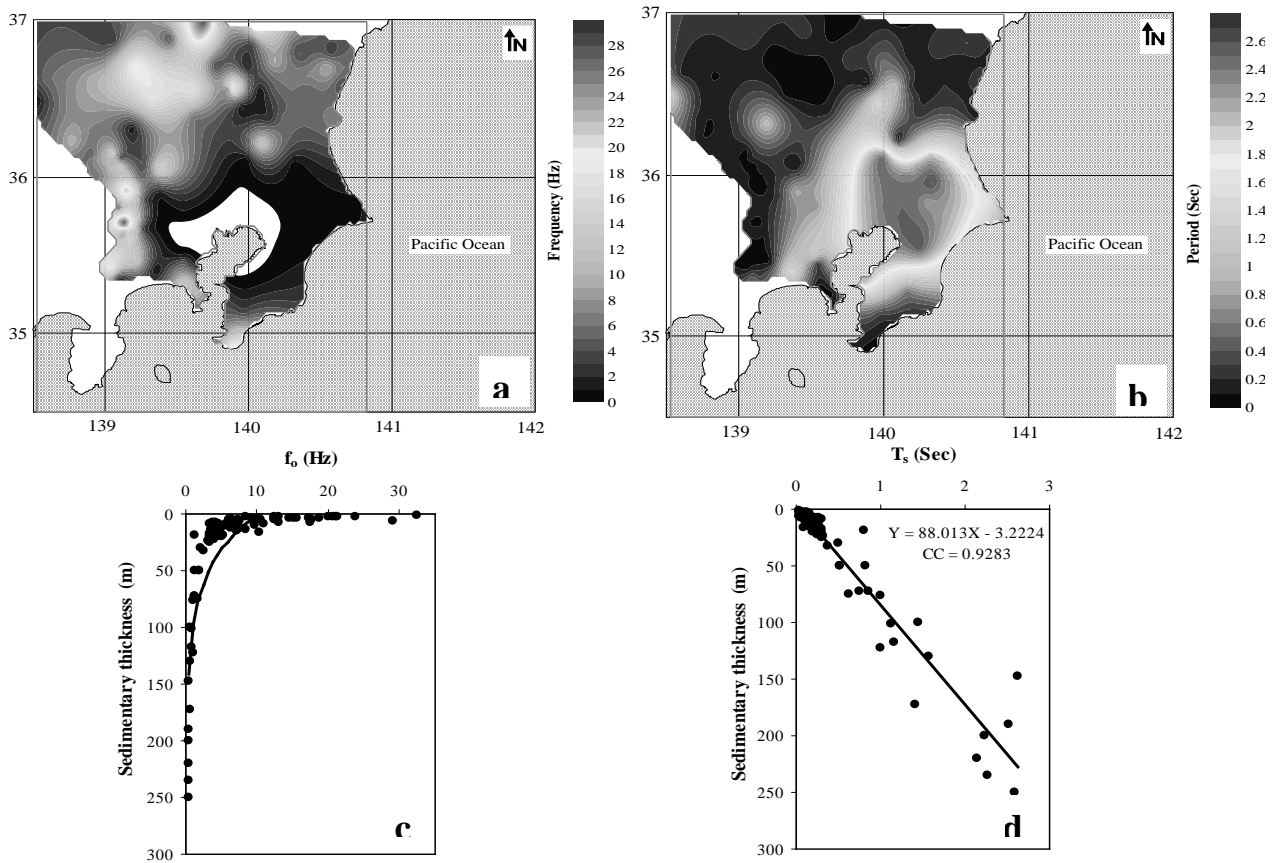


Fig. (5): a: Contour map illustrating the fundamental frequency (f_0) of the sedimentary cover. b: Contour map illustrating the characteristic site period (T_s) of the sedimentary cover. c: Relationship between the fundamental frequency (f_0) and the sedimentary thickness. d: Relationship between the characteristic site period (T_s) and the sedimentary thickness.

Density Gradient (D_i)

Adams (1951) introduced the quantitative form of the density gradient as:

$$D_i = \frac{\rho}{k} \quad (6)$$

where: (ρ) is the material density and (k) is the bulk modulus.

Stumpel *et al.* (1984) expressed the density gradient in terms of compressional and shear-wave velocities as:

$$D_i = \left(V_p^2 - \left[\frac{4}{3} \right] V_s^2 \right)^{-1} \quad (7)$$

In terms of the velocity-squared ratio (V_s^2/V_p^2), equation (7) can be written as:

$$V_p^2 D_i = \left(1 - \left(\frac{4}{3} \right) \left(\frac{V_s^2}{V_p^2} \right) \right)^{-1} \quad (8)$$

Abd El-Rahman (1991) expressed this equation in terms of the velocity-squared ratio as:

$$D_i = \left(\frac{3}{V_p^2} \right) - \left(4 \left(\frac{\mu}{E} \right) - 1 \right) = \left(\frac{3}{V_p^2} \right) - \left(\frac{(1-\sigma)}{(1+\sigma)} \right) \quad (9)$$

where: E is Young's modulus.

Cordier (1985) summarised the ranges of ($D_i \cdot V_{p2}$) corresponding to the degree of soil competence (Table 5). Equation (8) was used to calculate the density gradient ($D_i \cdot V_{p2}$) for the bedrock unit in the study area. The calculated density gradient ($D_i \cdot V_{p2}$) revealed values ranging from 1.01 to 2.54 (Fig. 8a). The northwestern area is characterised by relatively high ($D_i \cdot V_{p2}$) values, reflecting moderately competent material (Fig. 8b). For the soil cover, the calculated ($D_i \cdot V_{p2}$) displayed values ranging from 1.01 to 1.85 (Fig. 8c). MNT is characterised by relatively low ($D_i \cdot V_{p2}$) values, which are classified as non-competent, very soft soil, although towards the north-northwestern parts, the materials classification is ranged from non-competent, soft soil to fairly competent soil (Fig. 8d).

Stress Ratio (S_i)

During excess pressure caused by a stress change, consolidation settlement occurs. By the end of the consolidation process, the excess pressure is nearly zero

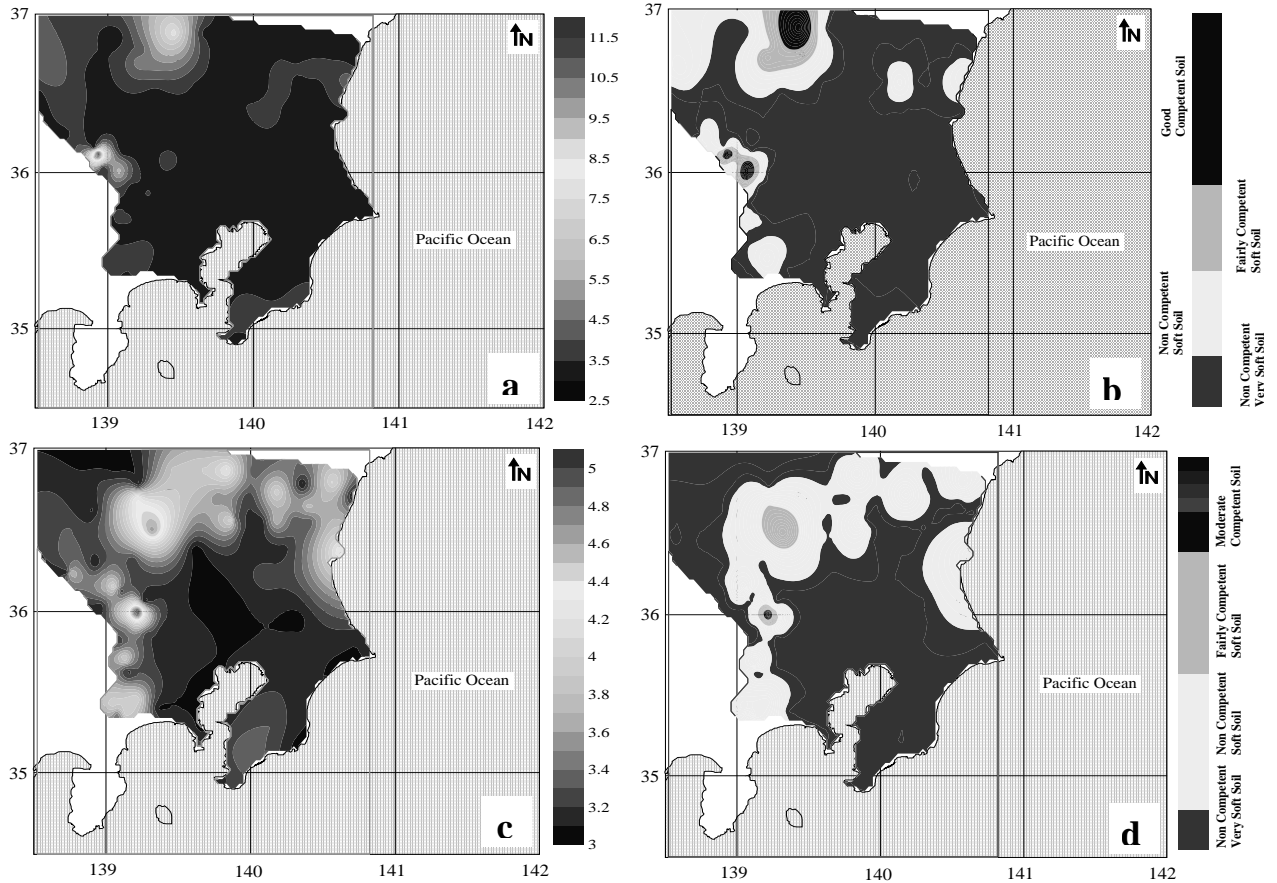


Fig. (6): a: Concentration Index lateral distribution for the bedrock. b: Concentration Index classification for the bedrock. c: Concentration Index lateral distribution for the sedimentary cover. d: Concentration Index classification for the sedimentary cover.

Table 2: Ranges of the concentration index and stress ratio that correspond to the soil competent degree, as described by Abd El-Rahman (1989).

	Weak		Fair		Good
	Incompetent		Fairly competent		Competent
	Very soft	Soft	Fairly compacted	Moderately Compacted	Compacted
Concentration Index C_i	3.5–4.0	4.0–4.5	4.5–5.0	5.0–5.5	5.5–6.0
Stress Ratio S_i	0.7–0.61	0.61–0.52	0.52–0.43	0.43–0.34	0.34–0.25

Table 3: Poisson's Ratio (σ), Rigidity (μ), and Material Index (γ) corresponding to different material, according to Birch (1966), Gassman (1973), Tatham (1982) and Sheriff and Geldart (1986).

Rock sample	σ	μ	γ
Liquids	0.5	0	-1
Perfect elastic rocks	0.25	$\mu = \lambda$	0
Very hard indurated rocks	0.00	$\lambda = 0$	+1

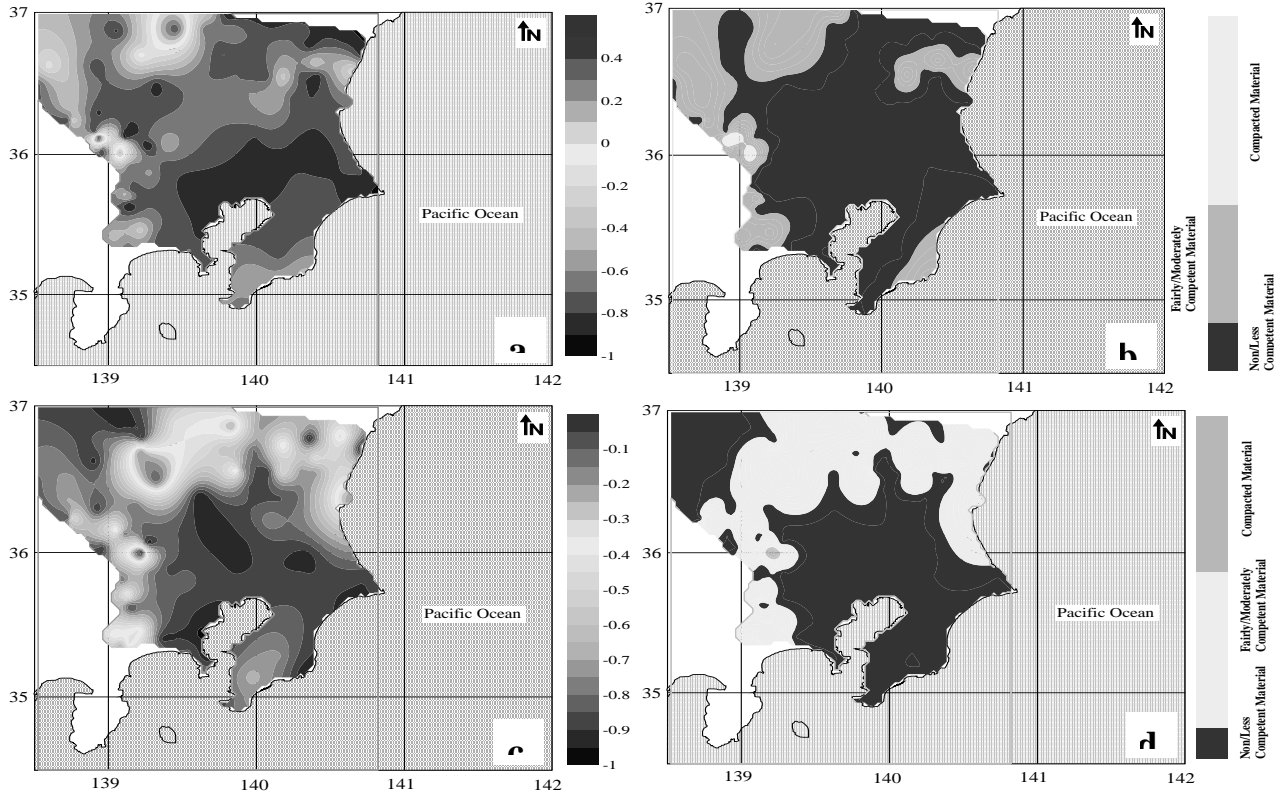


Fig. (7): a: Material Index lateral distribution for the bedrock. b: Material Index classification for the bedrock. c: Material Index lateral distribution for the sedimentary cover. d: Material Index classification for the sedimentary cover.

Table 4: Soil description with respect to Poisson's ratio and material index, as described by Birch (1966), Gassman (1973), Tatham (1982) and Sheriff and Geldart (1986)

Soil	Incompetent	Fairly to	Competent	Very highly
description	to slightly	moderately	materials	competent
parameters	Competent	Competent		materials
Poisson's Ratio σ	0.41-0.49	0.35-0.27	0.25-0.16	0.12-0.03
Material Index γ	(-0.5)-(-1)	(-0.5)-(0.0)	0.0-0.5	>0.5

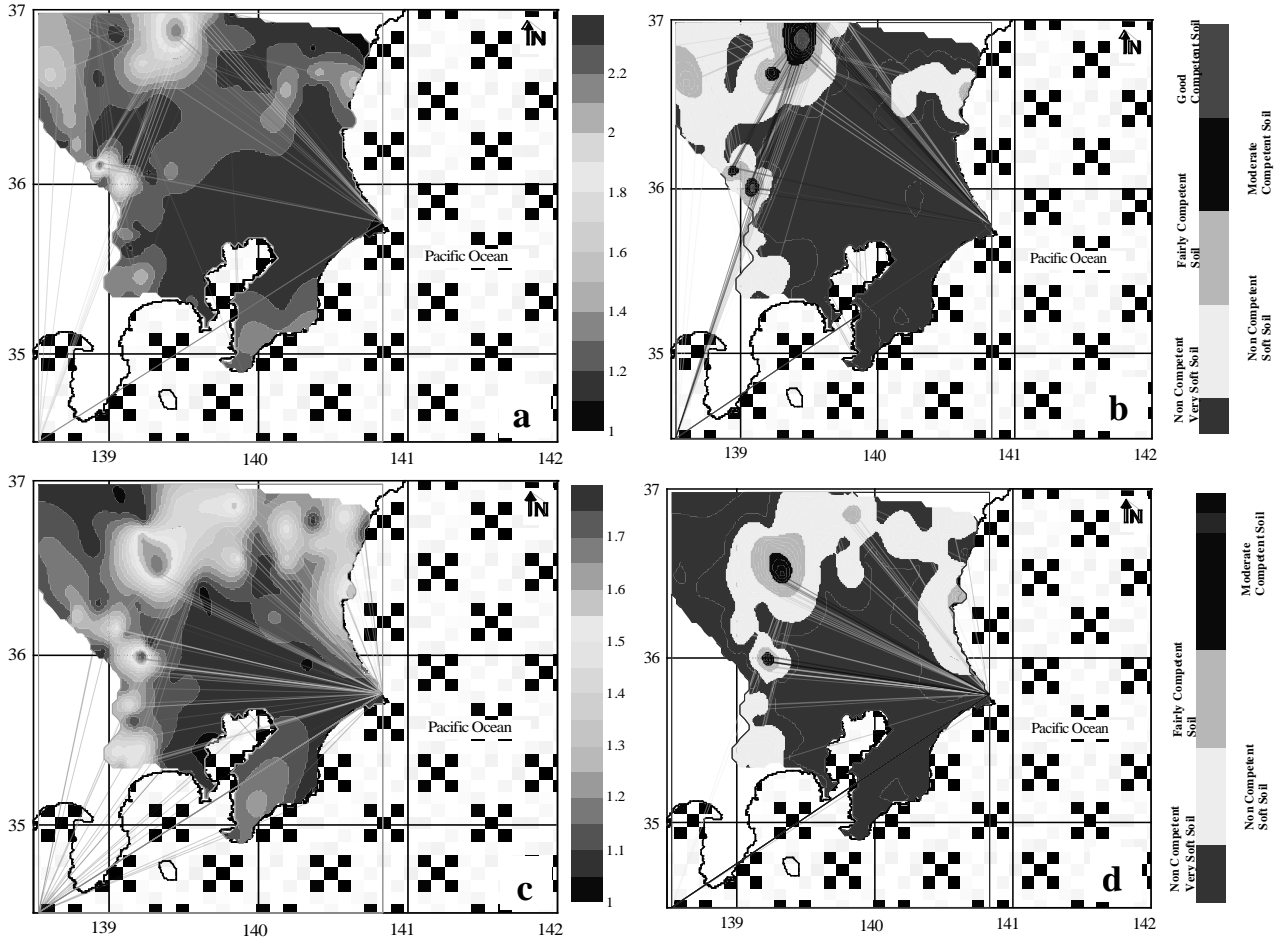


Fig. (8): a: Density Gradient ($D_i.V_{p2}$) lateral distribution for the bedrock. b: Density Gradient ($D_i.V_{p2}$) classification for the bedrock. c: Density Gradient ($D_i.V_{p2}$) lateral distribution for the sedimentary cover. d: Density Gradient ($D_i.V_{p2}$) classification for the sedimentary cover.

Table 5: Ranges of $D_i.V_{p2}$ corresponding to the degree of soil competence, according to Cordier (1985).

	Non competent		Fairly	Moderate	Good
	Very soft	Soft	competent	competent	Competent
$D_i.V_{p2}$	1.25–1.4	1.4–1.55	1.55–1.70	1.70–1.85	1.85–2.00

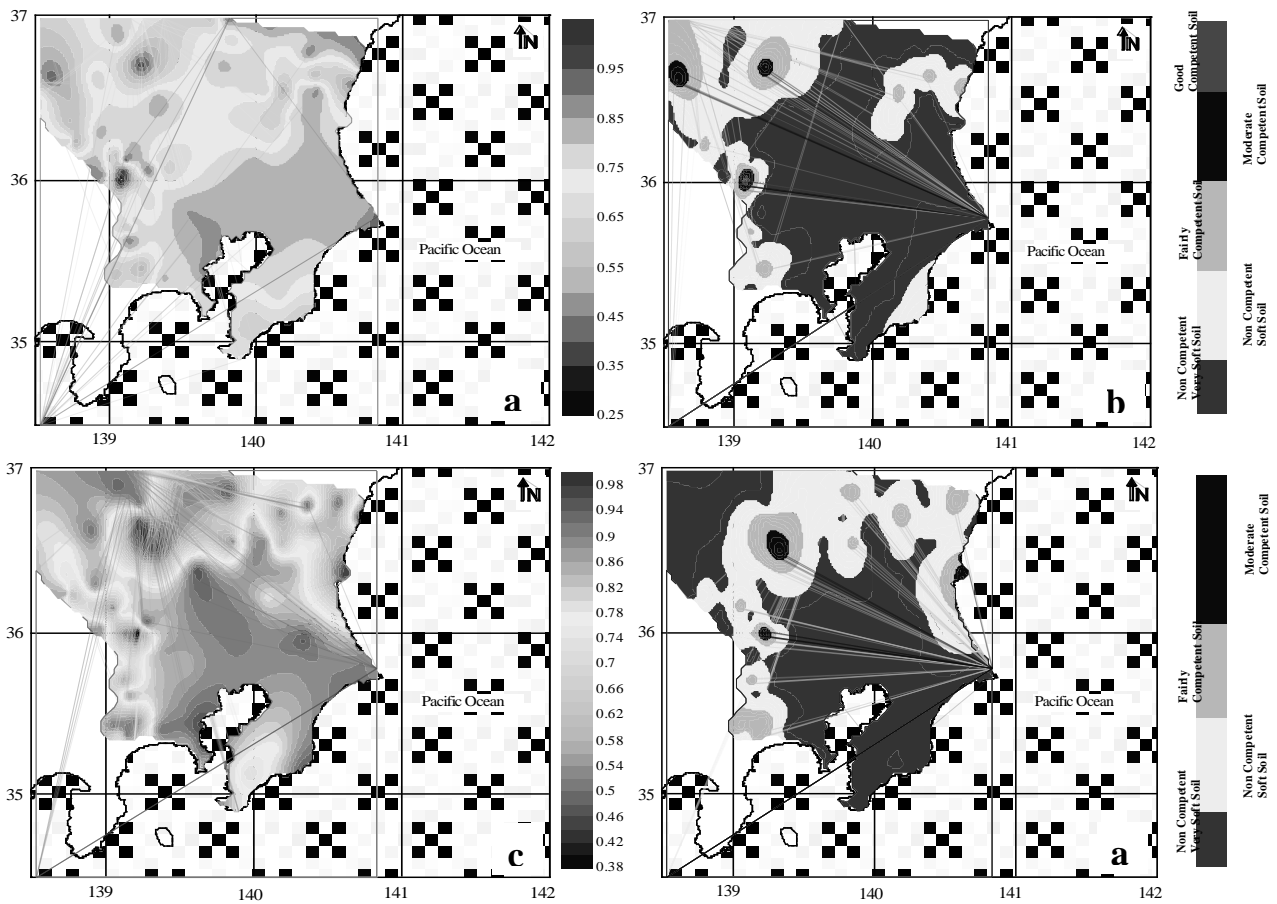


Fig. (9): a: Stress Ratio lateral distribution for the bedrock. b: Stress Ratio classification for the bedrock. c: Stress Ratio lateral distribution for the sedimentary cover. d: Stress Ratio classification for the sedimentary cover.

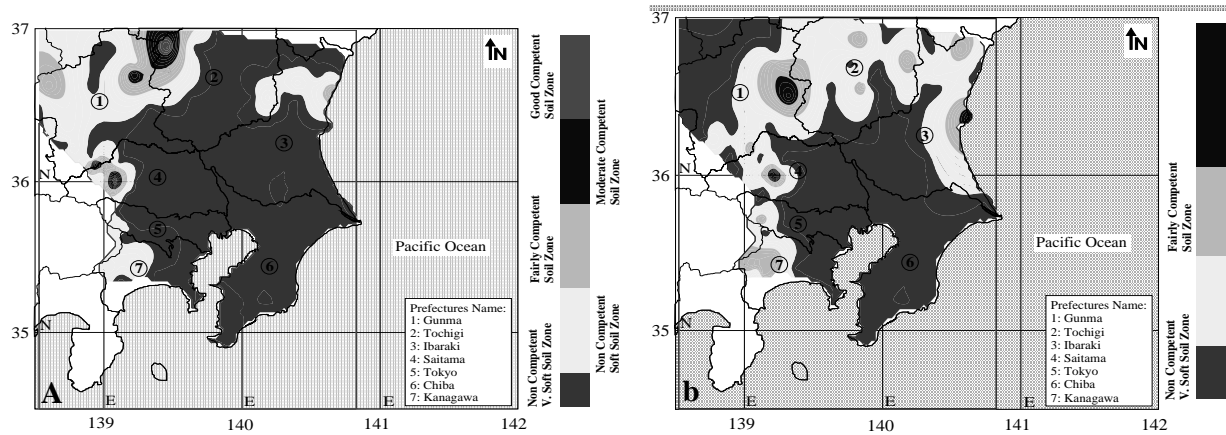


Fig. (10): a: Competence zones for the bedrock. b: Competence zones for the sedimentary cover.

and stress change will have changed from a total to an effective state. In this stress state, the soil state is defined as being in an equilibrium steady state condition of zero lateral and vertical strains (Bowles, 1982). Bowles (1982) pointed out that, there is a relationship between Poisson's ratio (σ) and stress ratio (S_i) for normally consolidated soils. This relationship was described by Bowles (1982) and Thomson (1986) as:

$$S_i = \frac{\sigma}{(1-\sigma)} \quad (10)$$

From several general observations about (S_i), Bowles (1982) pointed out that, S_i tends to be higher for fine soils than for coarse soils, that S_i is larger for loose cohesionless soils, that S_i tends to decrease with an increase in the overburden pressure, and that S_i is larger when the soil is over-consolidated. Abd El-Rahman (1991) pointed out the presence of a relationship between Poisson's ratio, S_i and P, S-wave velocities as:

$$S_i = 1 - 2\left(\frac{V_s^2}{V_p^2}\right) = (C_i - 1)^{-1} \quad (11)$$

Abd El-Rahman (1989) summarised the ranges of stress ratio (S_i) corresponding to soil competent degree (Table 2). In the study area, the calculated (S_i) for the bedrock layer revealed values ranging from 0.25 to 0.98 (Fig. 9a). The northwestern part is characterised by relatively high (S_i) values, which according to Abd El-Rahman (1989), reflect fairly competent to moderately competent soil (Fig. 9b). For the soil cover, the calculated (S_i) displayed values ranging from 0.31 to 0.98 (Fig. 9c). The Kanto basin is characterised by relatively low (S_i) values, which are classified as non-competent and very soft soil (Fig. 9d).

DISCUSSION

The study area is divided into zones according to the lateral variations in engineering parameters calculated for the bedrock and soil cover units (Fig. 10). The Kanto area is widely covered by Quaternary sediments at the Kanto basin, and this feature may affect the results obtained for the shallow layers. A geological map of the target region, reproduced from the Geological Survey of Japan (1992), is presented in Figure 1c. Although it is covered by Quaternary sediments due to the significant thickness of the sedimentary cover and deep depth of the bedrock in the Kanto basin (which includes the Ibaraki, Saitama, Tokyo, and Chiba prefectures), this area is classified as a non-competent and very soft soil zone (Fig. 10a). However, toward the north and northwest, the parts corresponding to mountainous areas (Fig. 1b & c) are classified as more competent, ranging from non-competent soft soil to moderately or good competent soil zones (Fig. 10b). Good correspondence is detected between the distribution zones with regard to the bedrock and soil cover units.

The gravity anomaly map in the study area, reproduced from Kono and Furuse (1989) (Fig. 4d), displayed low gravity anomalies in the Kanto basin (Boso Peninsula), as well as at the northwestern side towards the mountainous areas, and high gravity anomalies towards the northeastern side of the study area. Relatively good correspondence is observed in the bulk density distribution of the sedimentary cover in most of the areas, excluding some locations, such as the Boso Peninsula. Lack of correspondence in these areas may be related to the lack of log density data for the K-NET sites distributed in this area and to the empirical equations used to estimate the density values at the KiK-net sites, as well as to the interpolation process used to interpret the available density data (Fig. 4c).

CONCLUSION

This study proposes that, the K-NET and KiK-net are useful for evaluating the regional engineering parameters, yielding the following results:

- (1) The engineering parameters evaluated are highly concordant with the soil layer/bedrock system in the Kanto region. These results are confirmed by comparing the geological data and those of other previous studies evaluating the pre-Tertiary basement.
- (2) The Kanto basin, which includes the Ibaraki, Saitama, Tokyo and Chiba prefectures, is classified as a non-competent and very soft soil zone. However, toward the north and northwest, the parts corresponding to mountainous areas are classified as more competent zones, ranging from non-competent soft soil zones to moderately or good competent soil zones.
- (3) To avoid the lack of necessary data for calculation of the engineering parameters, more borehole information are needed, according to the requirements of the engineering codes for geotechnical studies. Depending on the type of construction, these requirements include the number of drilled boreholes per constructed area, minimum spacing between the drilled boreholes, and the depth of the drilled boreholes.

REFERENCES

- Adams, L.H., (1951):** Elastic Properties of Materials of the Earth's Crust. Internal Construction of the Earth (edited by Gutenberg). Dover publications, Inc., New York.
- Abd El-Rahman, M., (1989):** Evaluation of the kinetic elastic moduli of the surface materials and application to engineering geologic maps at Maba-Risabah area (Dhamar Province), Northern Yemen. *Egypt. J. Geol.* 33 (1– 2), 229–250.

- Abd El-Rahman, M., (1991):** The potential of absorption coefficient and seismic quality factor in delineating less sound foundation materials in Jabal Shib Az Sahara area, Northwest of Sanaa, Yemen Arab Republic. Egypt, M. E. R. C. Earth Sci., vol. 5. Ain Shams University, pp. 181–187.
- Aki, K., Richards, P.G., (1980):** Quantitative Seismology. W. H. Freeman & Co., San Francisco.
- Birch, F., (1966):** Handbook of physical constants. Geol. Soc. Amer. Men. 97, 613.
- Boore, D.M. (2007):** Some thoughts on relating density to velocity, (http://quake.wr.usgs.gov/~boore/daves_notes/daves_notes_on_relating_density_to_velocity_v1.2.pdf).
- Borcherdt, R.D., Gibss, J.F. (1976):** Effects of local geological conditions in the San Francisco bay region on ground motions and the intensities of the 1906 earthquake, Bulletin of Seismological Society of America, Vol. 66, No. 2, pp.467-500.
- Bowles, J.E., (1982):** Foundation Analysis and Design, 2nd Ed. McGraw-Hill International Book Company, London, p. 587.
- Cordier, J.P. (1985):** Velocities in refraction seismology-Reidel Publishing Company Holland, 276 p.
- EUROCODE-8-prEN1998-1-3, (2001):** Design provisions for earthquake resistance of structures. European Committee for Standardisation.
- Gardner, G.H.F., Gardner, L.W., Gregory, A.R., (1974):** Formation velocity and density-the diagnostic basics for stratigraphic traps, Geophysics 39, 770–780.
- Gassman, F., (1973):** Seismische Prospektion. Birkhaeuser Verlag, Stuttgart, p. 417.
- Geological Survey of Japan, (1992):** Geological Atlas of Japan. Asakura Publishing, Tokyo, 2nd ed., 26 pp.
- Ishida, M., (1992):** Geometry and relative motion of the Philippine Sea plate and Pacific plate beneath the Kanto-Tokai district, Japan, J. Geophys. Res. 97, 489–513.
- Joyner, W.B., Fumal, T.E., (1984):** Use of measured shear-wave velocity for predicting geologic and site effects on strong ground motion, Proc. 8th World Conference on Earthquake Engineering, Vol.2, pp.777-783.
- King, T.V.V., (1966):** Mapping organic contamination by detection of clay- organic processes. Proceeding AGWSE/NWWA/API.
- Kinoshita, S., Kyoshin Net (K-NET), (1998):** Seism. Res. Letters 69, 309-332.
- Kinoshita, S., Ogue, Y., (2002):** Site amplification of K-NET Sites in the Kanto Region, Central Japan. Seismotectonics in Convergent Plate Boundary, Eds. Y. Fujinawa and A. Yoshida, pp. 393-405.
- Koketsu, K., Higashi, S., (1992):** Three-dimensional topography of the sediment/basement interface in the Tokyo metropolitan area, central Japan. Bull. Seism. Soc. Am., 82, 2328-2349
- Komazawa, M., Hasegawa, I., (1988):** The graben structure suggested by gravimetric basement in the Kanto district, central Japan. Mem.Geol. Soc. Japan, no. 31, 57-74.
- Kono, Y., Furuse, N., (1989):** Gravity anomaly map in and around the Japanese islands. Univ. Tokyo Press, Tokyo, 76 pp.
- Kramer. S.L., (2004):** Geotechnical Earthquake Engineering, 2nd Ed. Pearson Education (Singapore) Pte. Ltd., Indian Branch, p. 653.
- Kulhawy, F.H., Trautmann, C.H., O'Rourke, T.D., (1991):** The Soil-Rock Boundary: What Is It and Where Is It?, Geotechnical Special Publication No. 28: Detection of and Construction at the Soil/Rock Interface, pp. 1-15.
- Midorikawa, S., Matsuoka, M., Sakugawa, K., (1994):** Site effects on strong-motion records observed during the 1987 Chiba-ken-tohooeki, Japan earthquake, Proc. 9th Japan Earthquake Engineering Symposium, Vol.3, pp.85-90.
- Okada, Y., Kasahara, K., (1990):** Earthquake of 1987, off Chiba, central Japan and possible triggering of eastern Tokyo earthquake of 1988, Tectonophysics 172, 351–364.
- Romanian code for the seismic design for buildings, (2006):** P100-1.
- Salem, H.S., (1990):** The theoretical and practical study of petrophysical, electric and elastic parameters of sediments. Germany, Kiel Insitut for geophysik. Ph.D. thesis.
- Sheriff, R.E., Geldart, L.P., (1986):** Exploration Seismology. Cambridge Univ. Press, Cambridge, p. 316.
- Sjogren, B., Ofsthus, A., Sandberg, J. (1979):** Seismic classification of rock mass qualities. Geophysical Prospecting. 27: pp. 409-442.
- Smith, W. H., Sandwell, D.T., (1997):** Global sea floor topography from satellite altimetry and ship depth soundings, *Science* 277, issue 5334.
- Stumpel, M., Kahler, S., Meissner, R., Nikereit, B., (1984):** The use of seismic shear waves and compressional waves for lithological problems of shallow sediments. Geophys. Prospect. 32, 662–675.

- Suzuki, H., (2002):** Underground geological structure beneath the Kanto Plain, Japan. Rep. Nat. Res. Inst. Earth Sci. Disaster Prevention, no. 63, 1-19.
- Tatham, R.H., (1982):** Vp/Vs and lithology. Geophysics 47 (3), 336-344.
- Toksoz, M.N., Cheng, C.H., Timur, A., (1976):** Velocities of seismic waves-porous rocks. Geophysics **41**, 6 21-6 45.
- Thomson, L., (1986):** Weak elastic anisotropy. Geophysics 1954-1966.
- Yamanaka, H., Yamada, N., (2002):** Estimation of 3D S-wave velocity model of deep sedimentary layers in Kanto plain, Japan, using microtremor array measurements. Butsuri-Tansa, **55**, 53-65.